RESEARCH ARTICLE



Wind-Tunnel Experiments of Turbulent Wind Fields over a Two-dimensional (2D) Steep Hill: Effects of the Stable Boundary Layer

Wei Zhang¹ · Corey D. Markfort² · Fernando Porté-Agel³

Received: 12 March 2023 / Accepted: 13 June 2023 / Published online: 13 July 2023 © The Author(s), under exclusive licence to Springer Nature B.V. 2023

Abstract

Flow separation caused by steep topography remains a significant obstacle in accurately predicting turbulent boundary-layer flows over complex terrain, despite the utilization of sophisticated numerical models. The addition of atmospheric thermal stability, in conjunction with steep topography, further complicates the determination of disrupted turbulent wind patterns. The turbulent separated flows over a two-dimensional (2D) steep hill under thermal stratification has not been extensively addressed in previous experimental studies. Such measurements are crucial for enhancing our comprehension of flow physics and validating numerical models. We measured the turbulent wind flows over a 2D steep hill immersed in a stable boundary layer (of the bulk Richardson Number $Ri_b = 0.256$) in a thermally-stratified boundary-layer wind tunnel. The flow separation, re-circulation zone and flow reattachment were characterized by the planar particle image velocimetry technique. Vertical profiles of mean air temperature and its fluctuations are also quantified at representative locations above the 2D steep hill and in the near wake region. Results indicate that the separated shear layer, initiated near the crest of the 2D steep hill, dominates the physical process leading to high turbulence levels and the turbulent kinetic energy production in the wake region for both stable and neutral thermal stability. Although the stable boundary layer does not dramatically change the turbulent flow pattern around the hill, the mean separation bubble is elongated by 13%, and its vertical extent is decreased by approximately 20%. Furthermore, the reduced turbulence intensities and turbulent kinetic energy of the near wake flow are attributed to the relatively low turbulence intensity and low momentum of the stable boundary layer due

Wei Zhang w.zhang13@csuohio.edu

Corey D. Markfort corey-markfort@uiowa.edu

Fernando Porté-Agel fernando.porte-agel@epfl.ch

- Mechanical Engineering Department, Cleveland State University, 1960 East 24th Street, Cleveland, OH 44115, USA
- ² Civil and Environmental Engineering, University of Iowa, Iowa City, IA 52242, USA
- School of Architecture, Civil and Environmental, Engineering École Polytechnique Fédérale de Lausanne, CH-1015 Lausanne, Switzerland



to buoyancy damping, compared to the neutral boundary layer. Additionally, a distinct low-temperature region—a cold pool—is extended beyond the separation bubble, reflecting the significant sheltering effect of the 2D steep hill on the downwind flow and temperature field.

Keywords 2D hill · Complex terrain · Thermal stability · Turbulent flows · Wind-tunnel tests

1 Introduction

Atmospheric boundary-layer (ABL) flow over complex terrain is of great interest for numerous practical applications, such as the evaluation of pollutant dispersion (Fernando 2010), aerodynamic loading on civil structures (Bitsuamlak et al. 2004), wind erosion and sediment transport for sea and dune morphological variations (Huang et al. 2018), wildfire prediction and hazard mitigation (Simpson et al. 2013), and prediction of local weather in mountainous or hilly areas (Chow et al. 2013). With the exponential growth of wind energy projects worldwide, the installation of wind farms spreads from flat and homogeneous regions to complex terrains. Placing wind turbines along ridges in hilly and mountainous areas takes advantage of terrain-induced high winds; however, it poses significant challenges to predicting power production, which is highly dependent on the local turbulent wind field. The variability of wind in space and time is recognized as a primary source of uncertainty in the wind industry. Errors of less than 1 ms⁻¹ of the mean wind speed in estimating the annual wind resources for a wind farm can result in multi-millions of dollars lost in annual revenues (Banta et al. 2013). Also, unsteadiness and high turbulence levels induced by flow separation in such complex terrain may substantially increase the structural loads on wind turbines and reduce turbine service lifespan. Reliable prediction of local turbulent wind fields over complex terrain is, therefore, essential for assessing wind resources and planning wind turbine micro-siting in wind energy applications.

Hills of a few kilometers in horizontal dimensions and maximum heights of a few hundred meters are typically submerged within an ABL. They have a significant impact on the flow field and affect the exchange of momentum, energy, and moisture between the atmosphere and the land surface (Athanassiadou and Castro 2001). Extensive studies on the ABL flow over hills with a gentle slope have been conducted in the framework of linear theory, assuming that the hill-induced perturbation on the flow is insignificant (Jackson and Hunt 1975; Hunt et al. 1988). The linear theory is very successful at predicting wind over gently sloping terrain and low hills (with a slope less than 10°, Kaimal and Finnigan (1994)) in neutral boundary layers, demonstrated by a favorable comparison to field observation data, such as that from the Askervein hill (Taylor and Teunissen 1987). However, a hill with a steep slope induces flow separation, leading to the prevalence of strong non-linear effects in the dynamics of the flow over the hill. Dramatic changes happen not only in the separated flow region but also over the whole flow field around the hill (Kaimal and Finnigan 1994). In this case, the linear theory breaks down and is no longer valid. Unlike flows around a bluff body with sharp edges (e.g., a rectangular prism, block, or cube) where the separation point is fixed, the onset of flow separation over a curved surface is sensitive to multiple factors, such as the specific geometry of the hill, surface roughness, inflow characteristics, and atmospheric thermal stability (Poggi and Katul 2007). The strength of each contributing factor and their interactions affect the subtle details of the complicated physical process. Hence, predicting



the onset of flow separation, the size of the separation bubble, and the generated turbulence is challenging for the ABL flows over a steep hill.

Along with the difficulty of predicting separated flows over steep topography, atmospheric thermal stability is another challenging parameter that requires careful consideration in wind prediction (Landberg et al. 2003). The thermal stability effect on the airflow in a diurnal cycle has recently attracted more attention from the wind energy community. In particular, as the wind turbine size keeps increasing, the vertical variation of wind shear closely associated with the atmospheric thermal stability becomes increasingly important in estimating power production and turbine fatigue load. The efficiency of a wind farm is generally higher in the convective boundary layers and lower in stable boundary layers (Porté-Agel et al. 2020). Wharton and Lundquist (2012) reported a difference of 15% in the average power output dependent on atmospheric stability in a West-coast North American wind farm. Wind-tunnel tests and computational studies, e.g., Markfort et al. (2012), Zhang et al. (2013), Hancock and Pascheke (2014), Abkar and Porté-Agel (2015), have examined the enhanced or suppressed wind-turbine wake recovery under the effects of atmospheric thermal stability over flat terrains. Howard et al. (2016) reported the response of a model wind turbine to the turbulence induced by the upwind topography under variable thermal stability. Large Eddy Simulation (LES) studies implemented with dynamic sub-grid scale models and the immersed boundary method have produced promising results of the turbulent wind flows over complex terrains coupled with various atmospheric stability, such as sinusoidal hills, rectangular blocks and urban street canopies (Wan et al. 2007; Wan and Porté-Agel 2011; Cheng and Porté-Agel 2013; Marjanovic et al. 2014).

To improve our capability to predict turbulent winds over steep topography, there is a need to understand the fundamental flow physics and obtain reliable datasets of sufficient spatial and temporal resolutions. Several field observation studies provide insights on flows over complex terrain, in particular, steep topography, including the Bolund experiment in Denmark (Berg et al. 2011; Bechmann et al. 2011), the MATERHORN field campaign (Fernando 2015), the Perdigão campaign in Portugal (Menke et al. 2020) and a case study of flow dynamics at a moderately complex terrain for wind farms (Wharton et al. 2015). However, field measurements of flow downwind of hills have been few, due to the cost of achieving good coverage of the flow separation region with the resolution essential for validating and verifying numerical results. The separation bubble typically covers a large area over the topography of interest—the height is comparable to the height of the hill, and the length is several times the hill's height. Furthermore, given the complexity of physical processes that occur concurrently in nature, interpreting field observation data often requires guidance from well-controlled laboratory studies that utilize scaled models (Fernando 2015; Hocut et al. 2015).

In laboratory studies, the majority of physical simulations have employed generic topography models with a well-defined geometry (e.g., Gaussian and sinusoidal hills) to examine key variables and important physical processes. For example, effects of varying steepness of a topography model in neutral boundary-layer flow are reported in Khurshudyan et al. (1981), Ayotte and Hughes (2004), Kanda et al. (2013). Upwind and local surface roughness changes on the mean flow and turbulent statistics (Cao and Tamura 2006, 2007) induced by a steep hill (Loureiro et al. 2007, 2008) are investigated. Experiments on turbulent flow responding to periodic hills were conducted by Gong et al. (1996), Rapp and Manhart (2011), Cierpka et al. (2013). Although theoretical and experimental studies of the stably-stratified flow over hills of shallow to moderate slopes were extensively conducted by Hunt and his colleagues (Britter et al. 1981; Hunt et al. 1996, 1997), there are only a handful of wind-tunnel studies on the turbulent wind flows over steep hills in thermally-stratified ABLs. Takahashi



et al. (2005) focused on turbulence statistics of the flow over a 3-D hill in the stable, neutral and unstable boundary layers. The results show that simulated thermal stability (Ri = 0.008 and -0.002) causes a marginal difference in the near wake downstream of the hill, which indicated the difficulty in achieving meaningful thermal stability conditions in wind-tunnel simulations. Ross et al. (2004) reported wind-tunnel measurements around a 2D steep hill in stable and neutral boundary layers and used experimental data to test the capabilities of various turbulence models; no information on the temperature field is provided in the wake. Houra and Nagano (2009) investigated the flow and thermal fields over a heated 2D steep hill for environmental problems in urban areas but in a relatively thin boundary layer, with the boundary layer thickness being half of the hill height. The limited results from carefully controlled wind-tunnel experiments have hindered our understanding of the underlying flow dynamics when steep topography and atmospheric thermal stability coexist.

The present wind-tunnel experiments were conducted to quantify and compare the turbulent flow pattern, temperature profiles, and turbulence statistics around a 2D steep hill that is immersed in a neutral and stable-stratified boundary layer. To improve our understanding of flow physics and facilitate Computational Fluid Dynamics (CFD) modeling efforts, we aim to answer specific questions as follows: (1) How does the stable boundary layer affect the mean flow speed-up ratio over the hill crest? (2) To what extent does the stable boundary layer affect the flow separation and reattachment of the steep topography? and (3) what is the effect on the turbulent flow properties around the 2D steep hill? We present wind-tunnel tests of the turbulent flow and thermal field over a 2D steep hill model in stable and neutral turbulent boundary layers and compare results with the available literature.

2 Flow Facility, Measurements and Inflow Conditions

2.1 Thermally-Stratified Boundary-Layer Wind Tunnel

Experiments were performed in the thermally-stratified boundary-layer (BL) wind tunnel at the Saint Anthony Falls Laboratory, University of Minnesota. The BL wind tunnel has a plan length of 37.5 m with a main test section fetch of 16 m and a cross-section of 1.7 m by 1.7 m. The turbulence intensity at the center of the wind tunnel is 2-4% for an approximately 2.0 ms⁻¹ free-stream wind speed. A heat exchanger was used to adjust the air temperature in the diffuser of the wind tunnel. The test-section floor consists of a series of heat exchangers made of smooth aluminum plates 0.3 m long and 25.4 mm thick in which a solution of 30% ethylene glycol was circulated. Electronic valves were installed to automatically set the desired temperatures of both the airflow and the test section floor via a Labview program. To produce conditions of neutral, stable or unstable thermal stratification, the temperature of the test section floor and the airflow can be independently controlled between 5 °C to 80 °C $(\pm 0.25 \,^{\circ}\text{C})$. Specifically, the stable boundary layer condition was generated by heating the air to $T_0 = 58$ °C and cooling the floor to $T_s = 8$ °C. For the neutral boundary layer, both air and the floor temperature were kept at 35 °C (\pm 0.25 °C). Similar wind-tunnel configuration and operation can be found in Carper and Porté-Agel (2008), Markfort et al. (2012) and Zhang et al. (2013). To simulate a rough surface, metallic chains of approximately 5 mm height were placed over the entire test section similar (Ohya 2001). The chains were aligned perpendicular to the flow direction and separated apart from each other by 0.20 m. This setup allows roughness elements to reach the same temperature as that of the test section floor and achieve an overall consistent thermal effect.



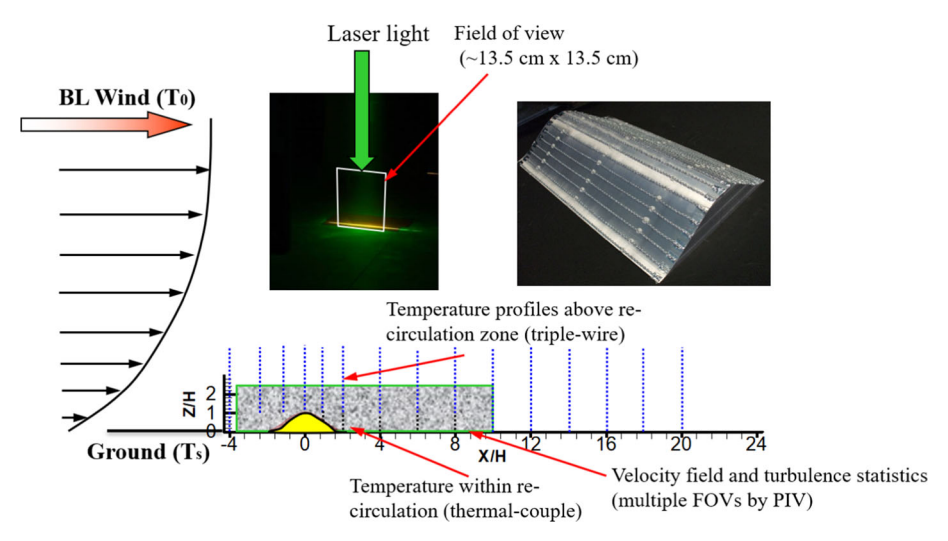


Fig. 1 Schematic diagram of the experimental set-up, coordinate system and measurement locations for flow and temperature. A sectional model of a 2D steep hill is shown in the inset

2.2 Two-dimensional (2D) Steep Hill Model

The profile of the 2D hill follows the cosine-squared function defined as:

$$Z = H\cos^2\left(\frac{\pi X}{L}\right), for - L/2 \le X \le L/2,\tag{1}$$

where H (= 0.07 m) is the hill crest height and L (= 0.145 m) is the distance from the crest to the foot (characteristic length, half-height point). The isolated 2D hill model of the same shape was used in Ross et al. (2004) and Cao and Tamura (2006), with the maximum slope (or steepness) of 0.73 (42°). In this study, the steep 2D hill model is placed normally to the incoming wind, occupying the whole span of the wind tunnel. The aspect ratio, the ratio of the spanwise length to the hill height, is 24 to minimize the side-wall effects of the wind tunnel (Barlow et al. 1999). The hill model was placed directly on the floor and fully immersed in the surface layer of the boundary layer ($H/\delta = 0.11$), yielding a negligible blockage ratio of approximately 4%. The boundary-layer thickness δ is the height where the mean wind speed reaches 99% of the free-stream wind speed. The 2D hill is made of aluminum to allow for temperature uniformity over the model surface through heat conduction, monitored by several thermal couples. Measurements of turbulent flow and thermal field were performed at the center line of the 2D hill model (Y/H = 0, Fig. 1). The metallic chains of 0.002 m high were attached with a spacing of 0.02 m on the surface of the hill to create a rough surface.

2.3 Measurement Techniques

We used a planar 2D two-component (2C) Particle Image Velocimetry (PIV) system (TSI, Inc.) to measure the flow field around the 2D steep hill, in the region of X/H = -3.5 to 8.5 and Z/H = 0 to 1.95, where flow separation is expected to occur and the flow is highly turbulent (Fig. 1). The PIV light sheet is created by using a Nd: YAG pulsed laser (Quantel USA) with $\lambda = 532$ nm and 190 mJ/pulse. Olive oil droplets, of a mean diameter of about $1\mu m$,



were atomized with six Laskin nozzles to seed the flow. A Powerview Plus 4MP 12-bit CCD camera captured particle images at 1.4 Hz with the resolution of 2048×2048 pixels². Particle images were acquired with the field of view (FOV) of 135×135 mm² at the largest aperture setting of f#2.8 and a 105 mm lens. The corresponding physical resolution is about 2.3 mm. A thin layer of fluorescent paint was carefully applied on the floor surface to minimize the reflection of laser light from the wind-tunnel roof.

Particle images were pre-processed by subtracting the background image to improve the signal-to-noise ratio. An iterative multi-grid cross-correlation method with second-order accuracy was utilized to acquire instantaneous velocity fields (Raffel et al. 2018). The final interrogation window used was 32×32 pixels² with 50% overlapping (INSIGHT3G, TSI). Erroneous velocity vectors, less than 1% of the total calculated vectors, were replaced by vectors interpolated from valid neighboring vectors through a Gaussian scheme. The measurement uncertainty of the instantaneous velocity vectors is estimated to be within 2%. The mean velocity field (U, W) was obtained by ensemble-averaging 3000 instantaneous velocity fields (u, w). The fluctuating components (u', w'), derived by subtracting the mean velocity from the instantaneous velocities, were used to compute turbulence intensities, turbulent kinetic energy and the Reynolds shear stresses. To cover the targeted flow region around the hill model, particle images of nine FOVs were obtained and ensemble-averaged results carefully stitched together.

In addition to the PIV measurements, a customized triple-wire (combination of a cross-wire and a cold-wire) is used to measure the vertical profiles of instantaneous temperature at selected stream-wise locations outside the recirculation zone (Fig. 1). This anemometer has been employed to quantify turbulent momentum and heat fluxes of thermally-stratified boundary-layer flows in previous studies, but it cannot provide reliable measurements in reversed flows. The configuration of the anemometer, pre- and post- calibration as well as the measurement accuracy, can be found in Zhang et al. (2013). Additionally, a thermal couple was used to record temperature profiles in regions where the triple-wire measurements were not valid so that the mean temperature in the reversed flow could be retrieved.

2.4 Characteristics of the Neutral and Stable Boundary Layers

Experiments were carried out in both neutrally and stably stratified boundary layers. The bulk Richardson number is used to quantify the thermal stability, defined by:

$$Ri_b = (g/\overline{\theta})\delta\Delta T/U_0^2, \tag{2}$$

where ΔT is the difference between the free-stream temperature T_0 and the surface temperature T_s . Both T_0 and T_s were continuously monitored by thermal couples and adjusted as needed to maintain a consistent temperature difference ΔT of 50 °C for the stable boundary layer. Additionally, the free-stream velocity ΔU was measured using a pitot-tube above the boundary layer. δ is the nominal boundary layer thickness and $\overline{\theta}$ is the mean potential temperature. The Reynolds number based on the free-stream wind speed U_0 , the boundary-layer thickness δ and the air kinematic viscosity ν is:

$$Re_{\delta} = U_0 \delta / \nu.$$
 (3)

It is well known that the Reynolds number achieved in wind-tunnel tests is usually three orders of magnitude less than that in field studies. For thermally-stratified BL flow simulation, a Richardson number Ri_b is used for dynamic similarity. At a given temperature gradient or bulk temperature difference ΔT constrained by the heating and cooling capacity of the



facility (Sect. 2.1), the requirement for a lower free-stream speed U_0 to achieve a larger Ri_b contradicts the need for a higher U_0 to attain a greater Re (Finnigan et al. 2020). As a compromise, we set U_0 at approximately 2 ms⁻¹, which yields a Ri_b of 0.256, just beyond the critical value of $Ri_b = 0.25$ for a stable BL (Wood 1970). Also, U_0 is held at the level to achieve a similar Re in the neutral BL case, allowing for a fair comparison of the two cases. Similar experimental conditions were implemented by Howard et al. (2016).

In addition, the Brunt-Väisälä or buoyancy frequency N (Eq. 4) is estimated for the stable BL (Eq. 4). From Z=0 up to the height of the hilltop, N ranges from 2 to 4 Hz. The Froude number, based on two characteristic length scales Fr_L and Fr_H (Eqs. 5 and 6) fall in the range of 1.5–3.4 and 3.2–6.9, respectively. Combining with that $\frac{u_*}{NH}$ is less than 1, therefore, the obtained thermal stability condition is classified as weakly stable (Kaimal and Finnigan 1994) without gravity wave effects:

$$N = \sqrt{\left(\frac{g}{\overline{\theta}} \frac{\partial \overline{\theta}}{\partial Z}\right)},\tag{4}$$

$$Fr_L = \frac{U}{NL},\tag{5}$$

$$Fr_H = \frac{U}{NH}. (6)$$

The incoming neutral and stable boundary layers were characterized at the center line of the test section. Parameters of thermal and flow characteristics are summarized in Table 1. The boundary-layer thickness δ of both the neutral and the stable boundary layers is roughly 0.60 m where the streamwise velocity reaches 99% of the free-stream velocity. By fitting the surface-layer mean velocity profile, the effective roughness length z_0 and the friction velocity u_* were determined for the NBL inflow. For the SBL case, u_* was calculated using the maximum Reynolds shear stress near the surface.

The momentum thickness Θ , a measure of the momentum deficit in a boundary-layer flow, is estimated by:

$$\Theta = \int_0^\delta \frac{\rho(Z)}{\rho_0} \frac{U(Z)}{U_0} \left(1 - \frac{U(Z)}{U_0} \right) dZ,\tag{7}$$

where ρ_0 and U_0 are air density and mean velocity of the free-stream flow. Θ is 17% larger for the stable BL than that of the neutral BL case, indicating a substantially lower momentum in the stable BL. While the vertical profiles of the mean stream-wise velocity are similar for both cases (Fig. 2a), the turbulence intensity distribution demonstrates a clear difference in Fig. 2b. The maximum turbulence intensity for the neutral boundary layer is about 12%, while it is reduced to 9% in the stable boundary layer. The normalized temperature profile (in Fig. 2c) shows that the largest thermal gradient is near the surface and it decreases away from the surface.

3 Results and Discussion

3.1 Mean Flow Speed-up Over the Hill

Typical behavior of the mean flow field around the 2D steep hill is the streamwise velocity speed-up over the hill crest (Fig. 3) and the vertical deflection as the flow approaches the hill



 Table 1 Characteristics of the neutral and stable boundary-layer flows

Case	Surface temp θ_s (°C)	Air temp θ_0 (°C)	Roughness length z ₀ (mm)	Friction velocity $u_* \text{ (ms}^{-1}\text{)}$	Momentum thickness ⊖ (mm)	$Re_{\delta} = U_0 \delta / \nu$	$Re_* = u_* z_o / \nu$	Ri_b
NBL	35	35	7:0	0.089	49.3	7.4×10^4	4.0	ı
SBL	8	28	0.5	0.07	59.1	7.9×10^4	2.2	0.256



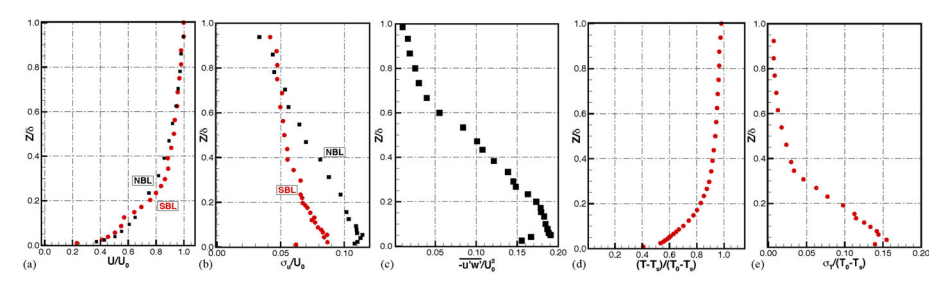
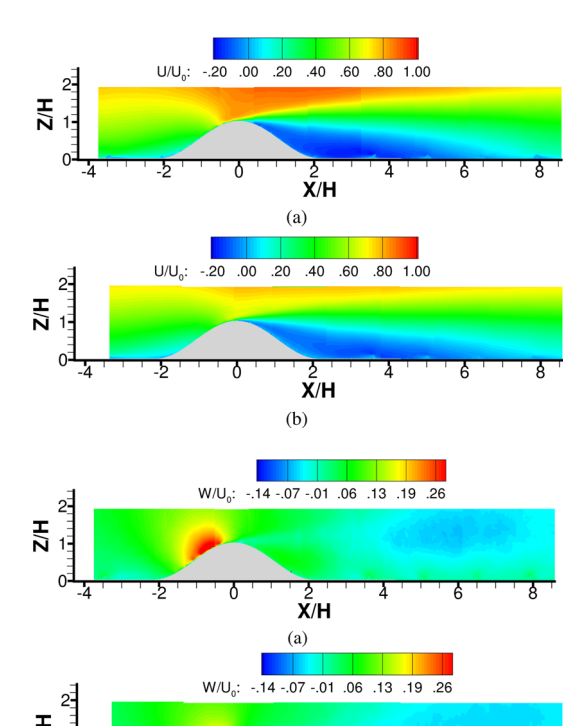


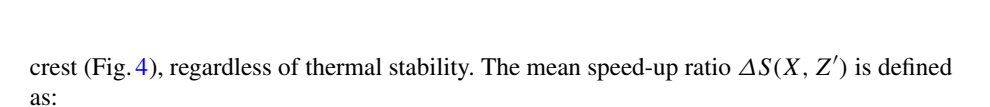
Fig. 2 Inflow characteristics of the neutral and stable BLs. **a** Vertical profiles of the mean stream-wise velocity; **b** Vertical profiles of the stream-wise turbulence intensity; **c** Vertical profile of Reynolds shear stress of the NBL; **d** Vertical profile of the normalized mean air temperature of the SBL; and **e** Vertical profile of the air temperature fluctuation of the SBL

Fig. 3 Contours of the mean stream-wise velocity U/U_0 around the 2D steep hill. a Neutral BL and b Stable BL



X/H(b)

Fig. 4 Contours of the mean vertical velocity W/U_0 around the 2D steep hill. **a** Neutral BL. **b** Stable BL



$$\Delta S(X, Z') = \frac{U(X, Z') - U_0(Z')}{U_0(Z')},\tag{8}$$

where U(X, Z') is the mean stream-wise velocity at the height Z' above the local surface of the hill and $U_0(Z')$ the incoming wind speed at the same height above the flat surface (Kaimal and Finnigan 1994; Cao and Tamura 2006). While flow speed-up appears to occur in front



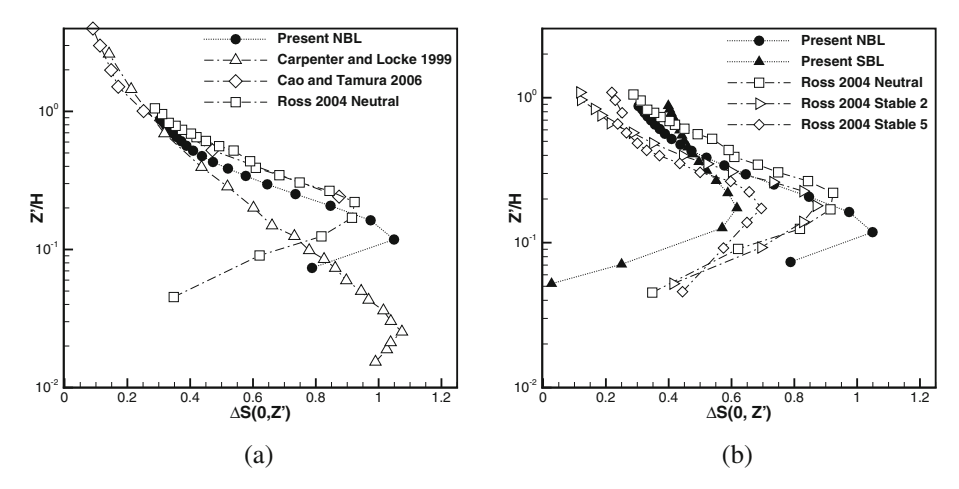


Fig. 5 Comparison of the speed-up ratio on the 2D steep hill crest with previous wind-tunnel results. a Neutral BL; b Stable BL

of the hill crest, it is a typical practice to quantify it right at the crest of the hill (Carpenter and Locke 1999; Safaei Pirooz and Flay 2018).

Vertical profiles of the speed-up ratio were compared with several wind-tunnel test results in the neutral boundary layer in Fig. 5a. One typical pattern is the rapid rise of the speed-up ratio from the surface, culminating in its peak value of ΔS_{max} , and then a gradual decrease as the height increases. In the present study, ΔS_{max} of 1.05 is observed at Z'/H = 0.1, which is consistent with the finding by Carpenter and Locke (1999), but greater than the values reported by Cao and Tamura (2006) and Ross et al. (2004). The difference is most noticeable at the height where the largest ΔS_{max} occurs. This discrepancy is likely associated with how close the velocity above the hill crest can be acquired by the particular measurement technique. Among the results shown here, Cao and Tamura (2006) did not capture enough data points near the surface to determine this location, while Carpenter and Locke (1999) reported the Z'/H = 0.02 - 0.03 for the largest ΔS_{max} .

To illuminate the effects of the stable stratification of the ABL on the speed-up ratio, the current results are compared with that of Ross et al. (2004) in Fig. 5b. The vertical profiles of the speed-up ratio follow a similar trend regardless of the thermal stability. However, ΔS_{max} is reduced by approximately 40% in the stable BL compared to that in the neutral BL. The less momentum of the approaching inflow (Table 1) may be attributed to the lower magnitude of the speed-up ratio in the stable BL case. The reduction of ΔS_{max} in stable BL cases is also clearly demonstrated in Ross et al. (2004). Despite the evident variation of the maximum speed-up ratio dependent on stability strength, the height corresponding to ΔS_{max} shifts upward slightly in the stable BL compared to the neutral BL case.

3.2 Mean Flow Separation and Reattachment

For a curved, natural hill with a steep slope, no solid theory can be readily applied to predict the exact location where the separation may be induced (Kaimal and Finnigan 1994). Given the velocity field, the zero wall shear stress indicates the flow separation point. Herein we use the location where the mean spanwise vorticity $2\omega_y$ defined by $\left(-\frac{\partial U}{\partial Z} + \frac{\partial W}{\partial X}\right)$ changes its sign at the surface to be the indicator of the onset of separation and the reattachment point.



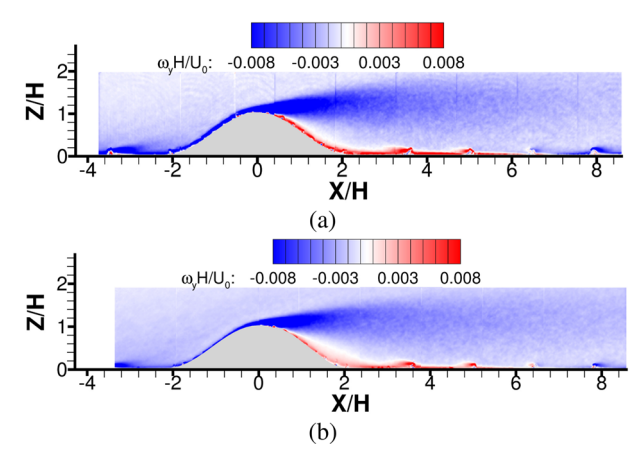
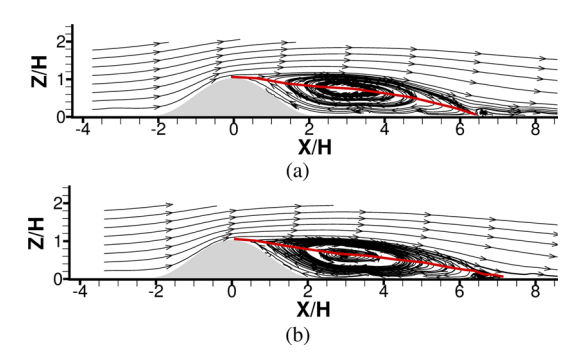


Fig. 6 Span-wise vorticity $(\omega_y H/U_0)$ contours of the flow over the 2D steep hill for **a** neutral and **b** stable BL cases

Fig. 7 Streamlines of the mean flow over the 2-D steep hill in a neutral and b stable BL cases. The red line marks the stagnation line U = 0 through the separation bubble



In an attached boundary layer, the spanwise vorticity ω_y near the surface is negative because $\frac{\partial W}{\partial X} \simeq 0$ and $\frac{\partial U}{\partial Z} > 0$. As flow separates and the streamwise velocity U becomes negative, ω_y is positive. Figure 6shows that a thin layer of intense negative vorticity (in blue) is distributed over the windward surface as the flow remains attached until flow passes the hill crest. Flow separates slightly downwind of the crest in the neutral boundary layer case, i.e., at $X_s/H=0.5$, where vorticity changes from negative to positive sign (in red). The reattachment point at $X_r/H=6.4$ is determined by ω_y switching to negative again. In a similar manner, the onset of flow separation is at $X_s/H=0.39$ and reattachment at $X_r/H=7.1$ around the 2D steep hill for the stable BL case.

Mean flow streamlines can often be conveniently used to visualize the separation bubble (Fig. 7). The stagnation line (contour of U=0) passes through the separation bubble center and the dividing streamline marks the upper edge of the bubble. The separation bubble agrees with that identified by the vorticity distribution over the surface. The length of the separation bubble is estimated as 5.9 H in the neutral BL case. However, in the stable boundary layer, the separation bubble length is about 6.7 H-13% longer. Moreover, the vertical extent of the separation bubble is affected by stable stratification. In comparison to the center of the separation bubble at Z/H=0.8 in the neutral BL case, it shifts downward to Z/H=0.64 in the stable BL, an indicator of the suppression in the vertical direction.

Table 2 summarizes the length of the separation bubble measured for multiple laboratory



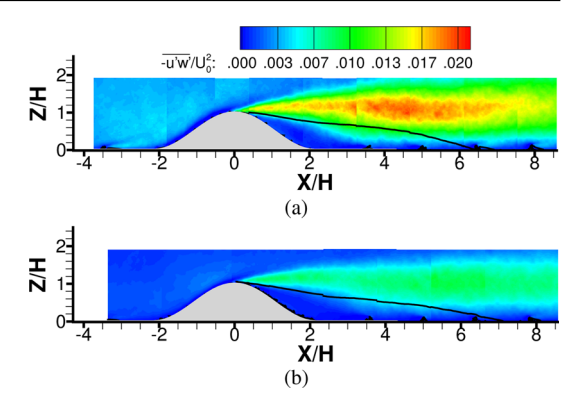
Table 2 Summary of 2D steep hill model geometry, the separation bubble length, and simulated boundary-layer flow conditions

Case description	Max. slope (°)	H/L	$\frac{X_S}{H}$	$\frac{X_r}{H}$	$\frac{(X_r - X_s)}{H}$	$\frac{\delta}{H}$	$Re_H \\ = U_0 H/\nu$	Thermal stratification
Almeida et al. (1993)	ı	I	0.43	4.82	4.4	^	6×10^4	Neutral
Houra and Nagano (2009)	I	0.4	0.5	6.0 ± 0.3	5.5 ± 0.3	0.5	2×10^4	Convective
Loureiro et al. (2007)	18.6°	I	0.5	6.67	6.17	1.67	2.8×10^3	Neutral
Kim et al. (1997) -S5H4	I	1.0	I	4.3 ± 0.3	I	3.6	3.3×10^4	Neutral
Kim et al. (1997) -S5H7	I	1.0	ı	5.25 ± 0.5	I	6.3	1.9×10^4	Neutral
Cao and Tamura (2006)	32°	I	1.25	6.5	5.25	6.25	1.05×10^4	Neutral
Huang et al. (2018)	31°	I	0.2	6.9	6.7	7.0	3×10^3	Neutral
Arya et al. (1987)	26°	I	8.0	6.3	5.5	8.0	2.8×10^4	Neutral
Present NBL	42°	0.48	0.5	6.4	5.9	9.8	8.1×10^3	Netural
Present SBL	42°	0.48	0.39	7.1	6.7	9.8	8.6×10^3	Stable

X_s is the separation point measured from the hill crest. X_r is the reattachment length. S5H4 and S5H7 refer to models of different hill heights in Kim et al. (1997)



Fig. 8 Contours of Reynolds shear stresses $\overline{-u'w'}/U_0^2$ of the flow over the 2-D steep hill in **a** neutral and **b** stable BL cases. The black line marks the stagnation line U=0 through the separation bubble



experiments investigating separated flow over a steep 2D hill. The table includes the slope of the tested 2D hill model as well as the inflow conditions to provide contextual information for the results. Despite all tested model hills being steep enough to induce flow separation, they differ significantly in slope. Additionally, depending on the boundary layer flow simulation and facilities, the ratio of the boundary layer thickness to hill height can vary greatly, ranging from 0.5 to over 8. Despite this variability, it is interesting to note that the separation bubble length consistently falls within the range of 5–7 H. Moreover, flow separation generally begins between 0.2H to 0.5H, depending on the flow conditions and hill geometry. The size of the separation bubble is sensitive to specific hill geometry, including surface roughness and boundary layer flow conditions, as previously reported by Kaimal and Finnigan (1994), and it is hard to generalize. It is worth noting that the Reynolds numbers in the laboratory are two to three orders of magnitude lower than those observed in the field. The atmospheric thermal stability is often not taken into account in laboratory tests.

While the current focus is on the mean flow separation and reattachment points, it is noted that the separated flow is dominated by large-scale, low-frequency unsteady turbulent motions. The onset of separation and reattachment location fluctuates spatially and temporally, which is also commented by Houra and Nagano (2009) and Huang et al. (2018).

3.3 Growth of the Separated Shear Layer

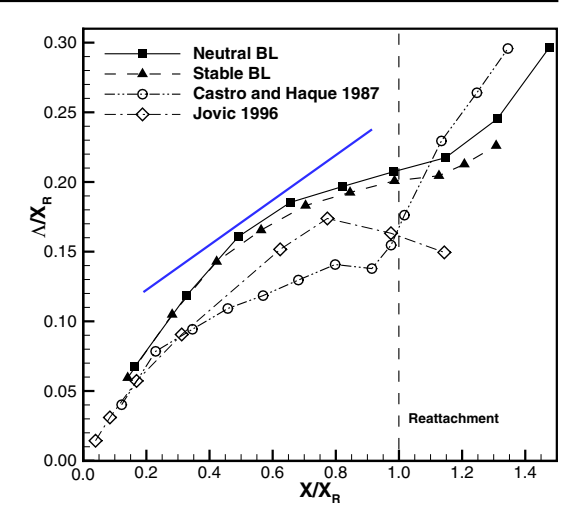
The separated shear layer initiated from the downwind of the 2D hill crest is the most salient flow structure that creates high turbulence levels and promotes turbulent mixing between the inner and outer flows. Figure 8 shows the distribution of Reynolds shear stress $(\overline{-u'w'}/U_0^2)$ of the flow over the 2D steep hill in both neutral and stable BL cases. In the neutral BL, a high magnitude of the Reynolds shear stress appears near the hill crest owing to the sharp velocity gradients between the speed-up region and the near-wake region. It further expands its extent until reaching a maximum at about X/H = 4.5. The stable BL produces a similar distribution of the Reynolds shear stress around the 2D hill, however, with a much lower magnitude indicating a suppressed momentum transport in the vertical direction.

The growth of the shear layer is measured by the increase in its vorticity thickness Λ , defined as:

$$\Lambda = \frac{\Delta U}{(\partial U/\partial Z)_{max}},\tag{9}$$



Fig. 9 Growth of vorticity thickness Λ in the neutral and stable boundary layers. The straight line (arbitrary origin) is the vorticity thickness growth of a plane mixing layer



where $\Delta U = U_{max} - U_{min}$, the difference between U_{max} and U_{min} the maximum and minimum velocities on the higher-speed side and the lower-speed side of the shear layer, and $(\partial U/\partial Z)_{max}$ is the local maximum of mean velocity shear. Figure 9compares the change of the vorticity thicknesses in the neutral and stable BL cases. Two distinct features are observed: firstly, as a function of the downwind distance from the hill, the shear layer growth does not follow a linear trend as is the case for a plane mixing layer. Specifically, the growth of the shear layer appears to be faster at the initiation of the shear layer and the post-reattachment region (with a steep slope) than that of a plane mixing layer. The behavior of the vorticity thickness qualitatively agrees with that observed by Castro and Haque (1987) for the separated flow by a flat plate, where the reversed flow region is surrounded by a solid wall and the separated shear layer. The growth of the vorticity thickness is also compared with the separated shear layer from a backward-facing step (Jovic 1996). However, it should be remarked that the shear layer growth is subjected to sensitivity to specific boundary conditions, initial boundary layer shape, the turbulence level and the presence of periodic perturbations, therefore, a direct comparison needs to be carefully viewed (Buckles et al. 1984; Almeida et al. 1993). Secondly, up to $X/X_R = 0.45$ the vorticity thickness growth is almost identical in the neutral and stable BL cases. Beyond $X/X_R = 0.45$, the growth is constantly lower in the stable BL than that in the neutral BL case, indicating that the shear layer expansion is slightly suppressed in the SBL case due to the constrained vertical motion.

3.4 Turbulence Intensities

The separated shear layer is associated with a region of high magnitude of turbulence intensities σ_u/U_0 and σ_w/U_0 (Figs. 10 and 11). In the neutral BL case, the large area encompassing the high streamwise turbulence intensity begins near the crest of the hill and extends further downwind. While the high level of vertical turbulence intensity is present in the same region as that of the streamwise turbulence intensity, it is approximately one-third less intense. The maximum values of both are observed at x/H = 4–5. In the stable BL case, the turbulence intensities follow a similar distribution, while the magnitude is dramatically decreased.

Considering the high turbulence associated with the separated shear layer and the low turbulence dominated in the lower part of the recirculation bubble, we inspect the anisotropy



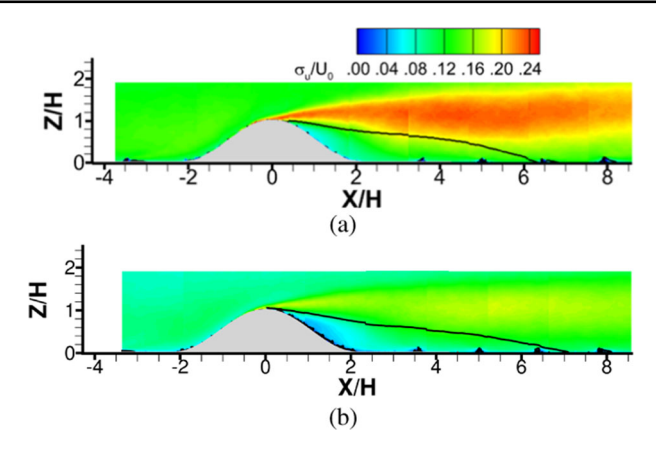


Fig. 10 Streamwise turbulence intensity σ_u/U_0 over the 2-D steep hill in **a** the neutral and **b** stable BL cases. The black line indicates the stagnation line of U=0 through the center of the recirculation bubble. The periodic near-surface peaks over the hill and ground (e.g., X/H=3.5, 5, 6.5, and 8) are U=0 contours illustrating small separation bubbles behind metallic chains

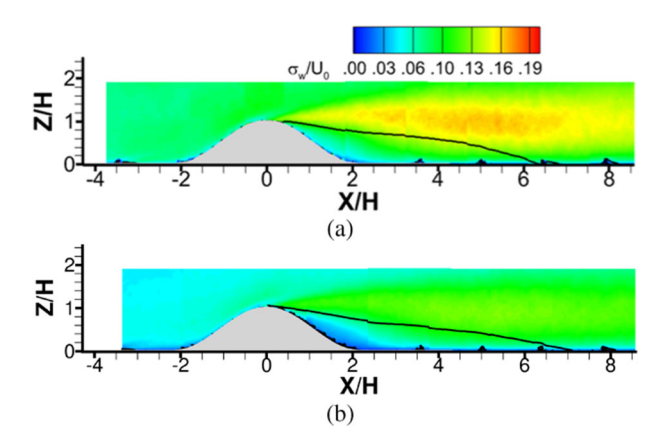


Fig. 11 Vertical turbulence intensity σ_w/U_0 over the 2-D steep hill in **a** the neutral and **b** stable BL cases. The black line indicates the stagnation line of U=0 through the center of the recirculation bubble and multiple small separation bubbles behind metallic chains

parameter, σ_w/σ_u , the ratio of the vertical to streamwise turbulence intensity (Fig. 12). A decrease in the anisotropy parameter corresponds to a greater disparity between the scales of the vertical and streamwise turbulent intensities, and therefore indicates a greater anisotropy (Calhoun et al. 2001). Overall the anisotropy parameter is less than unity in the flow over the 2D hill due to that values of σ_u/U_0 are consistently higher than those of σ_w/U_0 regardless of thermal stability, with the exception in the separation bubble zone, where the magnitude of the two normal stresses are similar. Upwind of the hill (X/H < -2) the magnitude of σ_w/σ_u is about 0.5, which is the typical feature of a surface layer developed over a homogeneous surface. As flow approaches the hill crest, a small region of high magnitude σ_w/σ_u is noted, above the initiation of the separated shear layer. On the lee side of the 2D hill the anisotropy parameter σ_w/σ_u displays the maximum value downwind of the separation point and the lower edge of the shear layer, close to unity. This indicates that while the center of the shear layer and the lower portion of the separation bubble (adjacent to the hill foot) are more



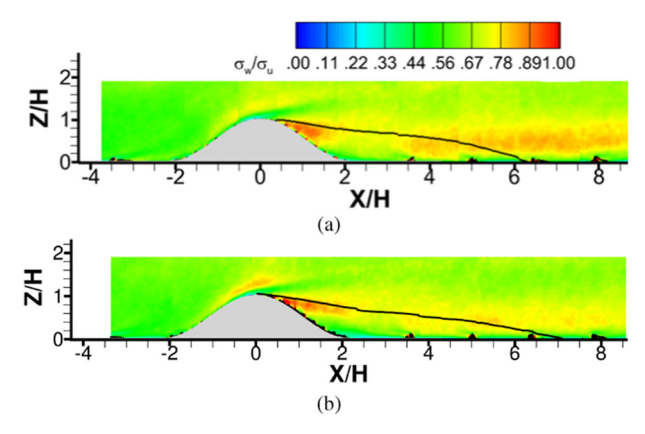


Fig. 12 Contours of the anisotropy parameter σ_w/σ_u of the flow over the 2-D steep hill in **a** the neutral and **b** stable BL cases. The black line indicates the stagnation line of U=0 through the center of the recirculation bubble and multiple small separation bubbles behind metallic chains

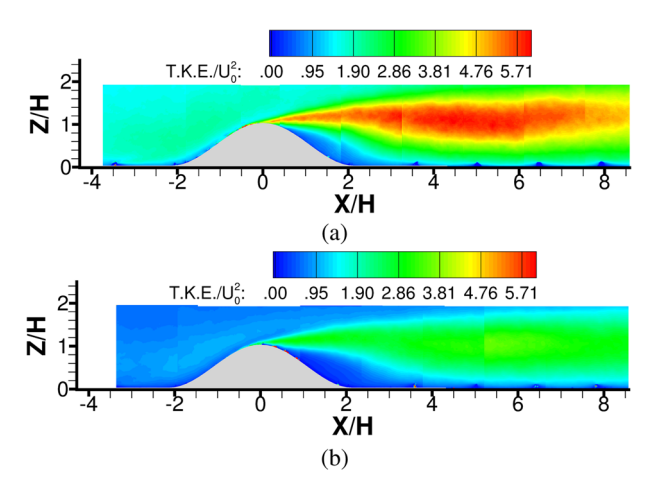


Fig. 13 Distribution of T.K.E of the flow over the 2D steep hill in a the neutral and b the stable BL cases

anisotropic, on the lower edge of the shear layer the scales of the vertical and streamwise turbulence intensities are similar. It is also noted that although turbulence intensities in the stable BL are considerably lower than that of the neutral BL case, the anisotropy parameters share the common feature of the highly spatial-varying distribution and are of comparable magnitude.

The turbulent kinetic energy (T.K.E) per unit mass of the flow over the 2-D steep hill is estimated with two measured velocity fluctuation components as follows:

$$T.K.E = \frac{1}{2}(\overline{u'^2} + \overline{w'^2}). \tag{10}$$

As shown in Fig. 13, the highest magnitude of T.K.E is in the central region of the separated shear layer for both cases. The effect of stable stratification is remarkable: the maximum T.K.E is reduced by half compared to that in the neutral BL, which is consistent with a pronounced reduction in turbulent intensities and Reynolds shear stress (Figs. 10, 11 and 8).



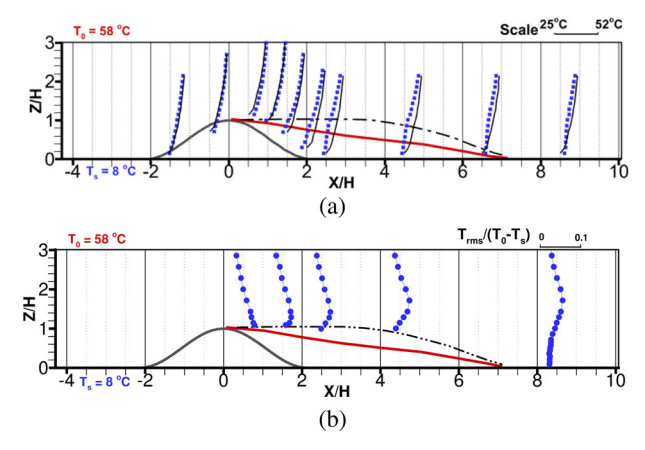


Fig. 14 Mean temperature profiles at selected locations in $\bf a$ compared against the temperature profile of the undisturbed stable BL inflow (vertical black lines), and temperature fluctuations in $\bf b$ over the 2D steep hill in the stable BL. The dashed black line indicates the edge of the bubble and the red stagnation line U=0 is through the separation bubble center

3.5 Temperature Profiles: Sheltering Effects from the Steep 2D Hill

A customized triple-wire (combination of a cross-wire and a cold-wire) is used to measure the vertical profiles of instantaneous temperature at selected stream-wise locations outside the recirculation zone. Mean temperature profiles over the 2-D hill from the local surface up to Z' = 2H in the stable BL are shown in Fig. 14. At the front foot of the hill (X = -2H) the temperature does not vary from the undisturbed SBL flow marked by solid black lines. The temperature is higher near the surface than the undisturbed SBL inflow as the flow speeds up and approaches the hill crest, where strong convection occurs. The more pronounced difference is found on the leeward side of the hill - the temperature is overall lower than that of the undisturbed SBL flow till the reattachment point. A "cold pool" forms downwind of the hill, which is unsurprising due to the almost stationary flow and weak turbulent mixing in the separation bubble. It reflects the significant sheltering effect of the steep topography over the downwind surface, which is discussed in Markfort et al. (2010, 2014). It is worth noting that the "cold pool" appears to be much larger than the separation bubble—at the outer edge of the bubble, the air temperature remains lower than the undisturbed SBL flow. For example, at X/H = 2 and 4, the reduced temperature can be seen up to 2H above the surface. In addition, profiles of temperature fluctuations normalized by $(T_0 - T_s)$ were shown in Fig. 14b. Recall that the triple-wire cannot provide valid measurements for reversed flows; only data points of temperature fluctuations above the recirculation zone are illustrated in Fig. 13b. On the leeward side of the hill crest, the peak of the temperature fluctuation occurs at a height beyond the edge of the separation bubble, which is linked to the expansion of the separated shear layer.

4 Conclusions and Outlook

This work reports measurements of turbulent flows and temperature distribution over a steep 2D hill in a thermally-controlled BL wind tunnel. The mean flow speed-up ratio, flow separation and reattachment, and the shear layer development was compared in the neutral and



stable BLs. The results obtained for the neutral boundary layer inflow are consistent with previous studies. However, this research presents new results on quantifying turbulent separated flows over a 2D steep hill in a stable boundary layer, which has not been extensively explored in prior work. The unique experimental datasets allow examining the separated turbulent boundary-layer flows subject to the coupled effects of the atmospheric thermal stability and an isolated steep topography.

The mean flow speed-up ratio over the crest of the 2D hill in the stable BL case is only half of that in the neutral BL, while the height where the maximum speed-up ratio occurs is only slightly affected. The mean velocity speed-up on the hilltop is of great interest both for wind energy engineers and civil engineers predicting wind loading on buildings and structures (Safaei Pirooz and Flay 2018). To maximize wind power production, the wind turbine rotor would be placed to catch the high wind near the crest. It has been shown that on the leeward side of a hill crest, the initiation of a separated shear layer leads to extremely high turbulence levels that can significantly impact the operation of a turbine.

The low momentum and the suppressed turbulence in the stable BL case are considered to induce an earlier onset of flow separation and a delayed reattachment, compared to that of the neutral BL conditions. The overall effect is that the separation bubble formed behind the 2D steep hill is elongated by about 13%, and suppressed by 20% in height than that in the neutral BL case. The separated shear layer undergoes a restricted growth and the T.K.E. of the near wake is remarkably reduced in the stable boundary-layer case. In addition, in the stable BL case, a low-temperature region (i.e., a cold pool) formed downwind of the steep 2D hill covers a larger height than the separation bubble, indicating the significant sheltering effect of the steep hill over the downwind surface.

The stable BL inflow demonstrates a clear effect on the turbulent separated flows induced by the 2D steep hill, even for a weakly stable stratification condition. It is important to highlight that the temperature gradient is consistently enforced in the approaching boundary-layer inflow. Additionally, the cooled ground surface and the 2D hill contribute to maintaining this temperature gradient. These conditions noticeably differ from previous studies, which simulated effects with either thermally-controlled flow conditions or utilized heated/cooled topography models exclusively (Houra and Nagano 2009). The present turbulent wind flow data of high-spatial resolution acquired in controlled wind-tunnel testings can be used to validate advanced numerical models, such as LES, for predicting turbulent wind fields over complex terrain. In the future, realizing a wider range of thermal stability conditions would be desirable to further our understanding of thermal stability effects on the separated BL flows over steep topography.

Acknowledgements This research was supported by the NSF CAREER Award 1944776 and NSF ATM-0854766, NASA Grant NNG06GE256 and the Swiss National Foundation Grant 200021-132122. The authors would like to express sincere gratitude to the anonymous reviewers for their insightful comments and suggestions that helped enhance the clarity and coherence of this paper.

Author Contributions WZ and CM conducted wind tunnel experiments. WZ analyzed the data and wrote the manuscript draft. FP conceptualized the topic and discussed the experimental plan. All authors provided funding sources, reviewed and revised the manuscript.

Funding The authors would like to thank the National Science Foundation ECI-1944776, ATM-0854766, NASA NNG06GE256 and the Swiss National Foundation Grant 200021-132122.

Data Availability All of the material is owned by the authors and/or no permissions are required. Datasets will be available upon request.



Declarations

Conflict of interest The authors have no competing interests as defined by Springer, or other interests that might be perceived to influence the results and/or discussion reported in this paper.

Ethical Approval Not applicable.

References

- Abkar M, Porté-Agel F (2015) Influence of atmospheric stability on wind-turbine wakes: a large-eddy simulation study. Phys Fluids 27(035):104
- Almeida GP, Duráo DFG, Heitor MV (1993) Wake flow behind two-dimensional model hills. Exp Therm Fluid Sci 7:87–101
- Arya SPS, Capuano M, Fagen L (1987) Some fluid modeling studies of flow and dispersion over two-dimensional low hills. Atmos Environ 4:753–764
- Athanassiadou M, Castro I (2001) Neutral flow over a series of rough hills: a laboratory experiment. Boundary Layer Meteorol 101(1):1–30
- Ayotte K, Hughes D (2004) Observation of bondary-layer wind-tunnel flow over isolated ridges of varying steepness and roughness. Boundary Layer Meteorol 112:525–556
- Banta R, Pichugina Y, Kelley N, Michael Hardesty R, Alan Brewer W (2013) Wind energy meteorology: insight into wind properties in the turbine-rotor layer of the atmosphere from high-resolution doppler lidar. Bull Am Meteor Soc 94:883–902
- Barlow JB, Rae WH, Pope A (1999) Low-speed wind tunnel testing. John Wiley & Sons, Hoboken
- Bechmann A, Sørensen NN, Berg J, Mann J, Réthoré P (2011) The bolund experiment, part II: blind comparison of microscale flow models. Boundary Layer Meteorol 141:245–271
- Berg J, Mann J, Bechmann A, Courtnery M, Jørgensen H (2011) The bolund experiment, part I: flow over a steep, three-dimensional hill. Boundary Layer Meteorol 141:219–243
- Bitsuamlak GT, Stathopoulos T, Bédard C (2004) Numerical evaluation of wind flow over complex terrain: review. J Aerosp Eng 17:135–145
- Britter RE, Hunt JCR, Richards KJ (1981) Air-flow over a two-dimensional hill—studies of velocity speed-up, roughness effects and turbulence. Q J R Meteorol Soc 107(451):91–110
- Buckles J, Hanaratty T, Adrain R (1984) Turbulent flow over large-amplitude wavy surfaces. J Fluid Mech 140:27-44
- Calhoun RJ, Street RL, Koseff JR (2001) Turbulent flow over a wavy surface: stratified case. J Geophys Resour 106:9295–9310
- Cao S, Tamura T (2006) Experimental study on roughness effects on turbulent boundary layer flow over a two-dimensional steep hill. J Wind Eng Ind Aerodyn 94(1):1–19. https://doi.org/10.1016/j.jweia.2005. 10.001
- Cao S, Tamura T (2007) Effects of roughness blocks on atmospheric boundary layer flow over a two-dimensional low hill with/without sudden roughness change. J Wind Eng Ind Aerodyn 95(8):679–695. https://doi.org/10.1016/j.jweia.2007.01.002
- Carpenter P, Locke N (1999) Investigation of wind speeds over multiple two-dimensional hills. J Wind Eng Ind Aerodyn 83:109–120
- Carper MA, Porté-Agel F (2008) Subfilter-scale fluxes over a surface roughness transition. Part I: measured fluxes and energy transfer rates. Boundary Layer Meteorol 126:157–179
- Castro IP, Haque A (1987) The structure of a turbulent shear layer bounding a separation region. J Fluid Mech 179:439–468
- Cheng WC, Porté-Agel F (2013) Evaluation of subgrid-scale models in large-eddy simulation of flow past a two-dimensional block. Int J Heat Fluid Flow 44:301–311
- Chow FK, De Wekker SF, Snyder BJ (2013) Mountain weather research and forecasting, recent progress and current challenges. Springer, Berlin
- Cierpka C, Scharnowski S, Manhart M, Káhler C (2013) On the significance of high spatial resolution to capture all relevant scales in the turbulent flow over periodic hills. Proceeding of the 10th international symposium on particle image velocimetry—PIV13, Delft, The Netherlands, 1–3 July, 2013
- Fernando HJS (2010) Fluid dynamics of urban atmospheres in complex terrain. Annu Rev Fluid Mech 42:365–389
- Fernando HJS (2015) The materhorn—unraveling the intricacies of mountain weather. Bull Am Meteor Soc 96:1945–1967



Finnigan J, Ayotte K, Harman I, Katul G, Oldroyd H, Patton E, Poggi D, Ross A, Taylor P (2020) Boundary-layer flow over complex topography. Boundary-Layer Meteorol 177:247–313

- Gong W, Taylor P, Dornbrack A (1996) Turbulent boundary-layer flow over fixed aerodynamically rough two-dimensional sinusoidal waves. J Fluid Mech 312(3):1–37
- Hancock P, Pascheke F (2014) Wind-tunnel simulation of the wake of a large wind turbine in a stable boundary layer: part2, the wake flow. Boundary Layer Meteorol 151:23–37
- Hocut CM, Liberzon D, Fernando HJS (2015) Separation of upslope ow over a uniform slope. J Fluid Mech 775:266–287
- Houra T, Nagano Y (2009) Turbulent heat and fluid flow over a two-dimensional hill. Flow Turbul Combust 83:389–406
- Howard K, Chamorro L, Guala M (2016) A comparative analysis on the response of a wind-turbine model to atmospheric and terrain effects. Boundary Layer Meteorol 158:229–255
- Huang G, Le Ribault D, Vinkovic I, Simoëns S (2018) Part I: a priori study of erosion and deposition with large eddy simulation of turbulent flow over multiple 2d sandy gaussian hills. Encycl Fluid Mech 18:581–609
- Hunt J, Shutts G, Derbyshire S (1996) Stably stratified flows in meteorology. Dyn Atmos Oceans 23(1–4):63–79
- Hunt J, Feng Y, Linden P, Greenslade M, Mobbs S (1997) Low-Froude-number stable flows past mountains. Nuovo Cimento Della Societa Italiana di Fisica C-Geophysics and Space Physics 20(3):261–272
- Hunt JCR, Leibovich S, Richards KJ (1988) Turblent shear flow over low hills. Q J R Meteorol Soc 114:1435– 1470
- Jackson PS, Hunt JCR (1975) Turblent wind flow over a low hill. Q J R Meteorol Soc 101:929-955
- Jovic S (1996) An experimental study of a separated/reattached flow behind a backforward-facing step. Re = 37000. NASA Technical Memorandum 110384
- Kaimal JK, Finnigan J (1994) Atmospheric boundary layer flows: their structure and measurement. Oxford University Press, Oxford
- Kanda I, Yamao Y, Wakamatsu S (2013) Particle-image velocimetry measurements of separation and re-attachement of airflow over two-dimensional hills with various slope angles and approach-flow characteristics. Boundary Layer Meteorol 179:439–468
- Khurshudyan L, Snyer W, Nekrasov I (1981) Flow and dispersion of pollutants over two-dimensional hills summary report on joint Soviet-American study. EPA-600/4-810067
- Kim HG, Lee CM, Lim HC, Kyong NH (1997) An experimental and numerical study on the flow over two-dimensional hills. J Wind Eng Ind Aerodyn 66:17–33
- Landberg L, Myllerup L, Rathmann O, Petersen EL, Jorgensen BH, Badger J, Mortensen NG (2003) Wind resource estimation—an overview. Wind Energy 6:261–271
- Loureiro JBR, Pinho FT, Freire APS (2007) Near wall characterization of the flow over a two-dimensional steep smooth hill. Exp Fluids 42(3):441–457. https://doi.org/10.1007/s00348-007-0252-z
- Loureiro JBR, Monteiro AS, Pinho FT, Freire APS (2008) Water-tank studies of separating flow over rough hills. Boundary Layer Meteorol 129(2):289–308. https://doi.org/10.1007/s10546-008-9314-x
- Marjanovic N, Wharton S, Chow FK (2014) Investigation of model parameters for high-resolution wind energy forcasting: case studies over simple and complex terrain. J Wind Eng Ind Aerodyn 134:10–24
- Markfort CD, Perez A, Thill J, Jaster D, Porté-Agel F, Stefan HG (2010) Wind sheltering of a lake by a tree canopy or bluff topography. Water Resour Res 46(W03):530
- Markfort CD, Zhang W, Porté-Agel F (2012) Turbulent flow and scalar flux through and over aligned and staggered wind farms. J Turbul 13:N30
- Markfort CD, Porté-Agel F, Stefan HG (2014) Canopy-wake dynamics and wind sheltering effects on earth surface fluxes. Environ Fluid Mech 14:663–697
- Menke R, Vasiljević N, Wagner J, Oncley SP, Mann J (2020) Multi-lidar wind resource mapping in complex terrain. Wind Energy Sci 5(3):1059–1073. https://doi.org/10.5194/wes-5-1059-2020
- Ohya Y (2001) Wind-tunnel study of atmospheric stable boundary layers over a rough surface. Boundary Layer Meteorol 98:57-82
- Poggi D, Katul G (2007) Turbulent flows on forested hilly terrain: the recirculation region. Q J R Meteorol Soc J Atmos Sci Appl Meteorol Phys Oceanogr 133(625):1027–1039
- Porté-Agel F, Bastankhah M, Shamsoddin S (2020) Wind-turbine and wind-farm flows: a review. Boundary Layer Meteorol 174(3):1–59
- Raffel M, Willert CE, Kompenhans J et al (2018) Particle image velocimetry: a practical guide, vol 3. Springer, Berlin
- Rapp C, Manhart M (2011) Flow over periodic hills: an experimental study. Exp Fluids 51:247–269
- Ross A, Arnold S, Vosper S, Mobbs S, Dixon N, Robins A (2004) A comparison of wind-tunnel experiments and numerical simulations of neutral and stratified flow over a hill. Boundary Layer Meteorol 113(3):427–459
- Safaei Pirooz AA, Flay RGJ (2018) Comparison of speed-up over hills derived from wind-tunnel experiments, wind-loading standards, and numerical modelling. Boundary Layer Meteorol 168:213–246



- Simpson CC, Sharples JJ, Evans JP, McCabe MF (2013) Large eddy simulation of atypical wildland fire spread on leeward slopes. Int J Wildland Fire 22(5):599–614
- Takahashi T, Kato S, Murakami S, Ooka R, Yassin M, Kono R (2005) Wind tunnel tests of effects of atmospheric stability on turbulent flow over a three-dimensional hill. J Wind Eng Ind Aerodyn 93(2):155–169. https://doi.org/10.1016/j.jweia.2004.11.003
- Taylor P, Teunissen H (1987) The Askervein hill project: overview and background data. Boundary-Layer Meteorol 39:15–39
- Wan F, Porté-Agel F (2011) Large-Eddy simulation of stably-stratified flow over a steep hill. Boundary Layer Meteorol 138(3):367–384
- Wan F, Porté-Agel F, Stoll R (2007) Evaluation of dynamic subgrid-scale models in large-eddy simulations of neutral turbulent flow over a two-dimensional sinusoidal hill. Atmos Environ 41(13):2719–2728. https://doi.org/10.1016/j.atmosenv.2006.11.054
- Wharton S, Lundquist JK (2012) Atmospheric stability affects wind turbine power collection. Environ Res Lett 7:014–005
- Wharton S, Newman JF, Qualley G, Miller WO (2015) Measuring turbine inflow with vertically-profiling lidar in complex terrain. J Wind Eng Ind Aerodyn 142:217–231
- Wood E (1970) Profile relationships: the log-linear range, and extensionn to strong stability. Q J R Meteorol Soc 96:67–90
- Zhang W, Markfort CD, Porté-Agel F (2013) Wind-turbine wakes in a convective boundary layer: a wind-tunnel study. Boundary Layer Meteorol 30:274–287

Publisher's Note Springer Nature remains neutral with regard to jurisdictional claims in published maps and institutional affiliations.

Springer Nature or its licensor (e.g. a society or other partner) holds exclusive rights to this article under a publishing agreement with the author(s) or other rightsholder(s); author self-archiving of the accepted manuscript version of this article is solely governed by the terms of such publishing agreement and applicable law

